Thin Solid Films 519 (2011) 7940–7946

Contents lists available at ScienceDirect

Thin Solid Films

journal homepage: www.elsevier.com/locate/tsf

Short communication

Investigation of thermomechanical responses in ultrafast laser heating of metal nanofilms

Zhiping Zhou, Wei Ma *

Institute of Mechanics, Chinese Academy of Sciences, Beijing 100190, China

ARTICLE INFO

Article history:
Received 12 April 2010
Received in revised form 19 May 2011
Accepted 23 May 2011
Available online 30 May 2011

Keywords:
Two-temperature model
Ultrafast laser
Thermomechanical response
Size effect
Nonequilibrium heating

ABSTRACT

The present work uses two-temperature model and Cattaneo's constitutive model to study the thermomechanical responses and the size effect on energy transport during ultrafast laser heating of Au nanofilms. It is shown that the grain size effects on thermophysical properties, heat transport and thermal stresses are rather evident when the average grain diameter is less than the electron mean free path. The study on heat transport shows that there are two heat waves propagating in the lattice during nonequilibrium heating of films. It is found that the classical thermoelastic theory can not reveal the generation of the ultrafast thermal stresses during nonequilibrium heating; however, it can approximately describe the stress evolution in the stage of thermal equilibrium.

1. Introduction

Interaction between ultrashort pulse laser and metallic nanostructures involves the nonequilibrium energy exchange between electrons and lattice [1–5] and the size effects [6–17] occurring in microscale energy transport processes. The nonequilibrium process occurs as the pulse width of the ultrashort pulse laser is comparable to the characteristic time for electrons to change their states. In the studies on nonequilibrium process, the energy exchange between electrons and the lattice was analyzed theoretically [1,2] and observed experimentally [3,4]. Two-temperature model [2] was used to describe the evolution of electron and lattice temperatures in the process of nonequilibrium heating of metal nanofilms. Two-temperature radiation heating model [5] was adopted to rigorously describe the hyperbolic nature of energy flux carried by electrons and the nonequilibrium energy exchange during ultrashort pulse laser heating of metal nanofilms.

The size effects are mainly studied at the specific microscopic scale and from the viewpoint of internal microstructure of materials, such as scattering of grain boundaries, crystal imperfections and other phonons, specular reflection of nanostructure surface and so on. Fuchs [6] and Sondheimer [7] (FS) investigated the surface scattering effect and the quantum effect of free electrons on electrical resistivity of thin metallic films. Subsequently, Mayadas and Shatzkes (MS) [8], based on experimental observations, [9] studied the grain boundary scattering on electric resistivity by extending FS theory. As a basic problem of microscale energy transport, the size effects on the electric resistivity of metallic nanostructures have been widely studied [10–17]. Since the thermal conductivity of metals is closely related to their electric conductivity [5,18], the size effect on thermal responses of metals is also an important problem in the field of microscale energy transport. In addition, the ultrashort pulse laser usually induces ultrafast mechanical responses in metals [1,4,19–25]. Thus, another important problem is the size effect on mechanical responses of nanostructures. Nowadays, ultrashort laser technique has been commercially available in microelectronic manufacture industry. Therefore, a better understanding of thermomechanical responses and size effects on the thermomechanical behaviors of nanostructures is useful for the improvement of laser technique.

Based on the two-temperature model and Cattaneo's thermal constitutive equation, this work carries out a simulation study on the thermomechanical responses during ultrafast laser heating of Au nanofilms. Size effects of the grain boundary scattering on the microscale energy transport are considered. The size effects on thermophysical properties and heat transport mechanisms are clearly exhibited. There are two heat waves propagating in the lattice during nonequilibrium heating of films. Classical thermoelastic theory can not reveal the generation of ultrafast thermal stresses during nonequilibrium heating; however, it can approximately describe the stress evolution in the stage of thermal equilibrium.

2. Theory

Ultrashort pulse laser heating of metal nanofilms involves three energy transport processes, i.e. the deposition of radiation energy on electrons, the energy exchange between electrons and the lattice, and the energy propagation through the media. Since the diameter of laser

* Corresponding author. Tel.: +86 01 82544238; fax: +86 01 62551238.
E-mail address: watwm@imech.ac.cn (W. Ma).

0040-6090/$ – see front matter © 2011 Elsevier B.V. All rights reserved.
doi:10.1016/j.tsf.2011.05.062

beam is much larger than the heat penetration depth, the process of ultrashort pulse laser heating of Au nanofilm can be modeled as a one-dimensional thermomechanical coupling problem, where the x axis is set normal to the film surface (Fig. 1). Therefore, the governing equations for the energy transport processes consist of the Cattaneo's constitutive equation for heat flux [26]

$$\tau_i \frac{\partial q}{\partial t} + q = -\kappa_i \frac{\partial T_i}{\partial x} \tag{1}$$

the two-temperature model for the energy balance of electron and the lattice [4,5]

$$\begin{aligned} C_e(T_e)\frac{\partial T_e}{\partial t} &= -\frac{\partial q_e}{\partial x} - G(T_e - T_l) + Q(x,t) \\ C\frac{\partial T_l}{\partial t} &= -\frac{\partial q_l}{\partial x} + G(T_e - T_l) - (3\lambda + 2\mu)aT_l\dot{\varepsilon}_{kk} \end{aligned} \tag{2}$$

the thermoelastic stress–strain relation

$$\sigma = (\lambda + 2\mu)\varepsilon - (3\lambda + 2\mu)\alpha(T_l - T_0) \tag{3}$$

and the thermoelastic kinetic equation

$$\rho\frac{\partial^2 u_x}{\partial t^2} = (\lambda + 2u)\frac{\partial^2 u_x}{\partial x^2} - (3\lambda + 2\mu)a\frac{\partial T_l}{\partial x} \tag{4}$$

In Eqs. (1)–(4), the quantities T, q, α, κ, ρ, u and ε_{kk} denote temperatures, heat flux, thermal expansive coefficient, thermal conductivity, density, film displacement component and volume strain of the lattice, respectively, and λ and μ stand for the Lamé constants. In Eq. (1), the subscripts $i = e$ and l denote *electron* and *lattice*, respectively. G is the electron–phonon coupling factor that governs the time scale for the electron and the lattice to reach thermal equilibrium. The relaxation time τ describes the background scattering due to combined effects of phonon and point defects. In the first relation of Eq. (2), the electron heat capacity C_e is proportional to the electron temperature $C_e(T_e) = C_{e0}T_e$, where C_{e0} is the electron specific heat constant at 300 K [18]. The laser source term $Q(x,t)$ is given as [5,20]

$$Q(x,t) = \sqrt{\frac{\beta}{\pi}}\frac{(1-R)J}{t_p\delta}\ exp\left[-\left(\frac{x}{\delta}\right) - \beta\left(\frac{t-2t_p}{t_p}\right)^2\right] \tag{5}$$

where J, t_p, δ and R are the laser fluence, the laser duration, the optical penetration depth and the reflectivity, respectively, and $\beta = 2.77$ is a given constant [5].

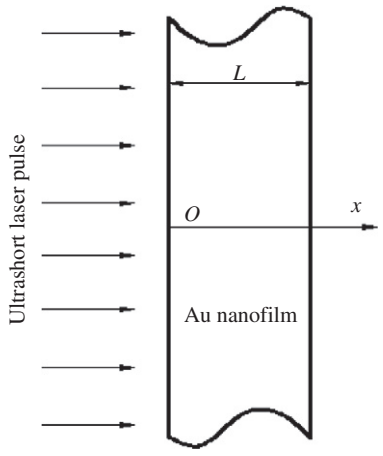

Fig. 1. One-dimensional thermomechanical analytic model of Au nanofilm heated by ultrashort laser pulse.

Before the laser irradiation, the film temperature is assumed to be equal to ambient temperature T_0 and both the normal stress component and that in the plane of films are free. During the radiation of laser, the film surfaces are assumed to be perfectly insulated and subjected to free normal stress conditions. Thus, the initial and boundary conditions are given as follows:

$$T_e(x,0) = T_l(x,0) = T_0,\ u_x(x,0) = \sigma_x(x,0) = \frac{\partial u_x(x,0)}{\partial t} = 0 \tag{6}$$

and

$$\frac{\partial T_e}{\partial x}(x,t) = \frac{\partial T_l}{\partial x}(x,t) = \sigma_x(x,t) = 0, (x = 0, L) \tag{7}$$

To study the size effects on the heat transport mechanisms, it is straightforward to obtain thermal conductivity of metals based on the electrical conductivity by using Wiedemann-Franz law [18]. The ratio of thermal conductivities between metallic film and bulk metal in FS model is

$$\frac{\kappa_f(T_e,T_l)}{\kappa_b(T_l)} = \frac{T_e}{T_l}\left[1 - \frac{3}{2b}(1-R_s)\int_1^\infty \left(\frac{1}{\xi^3} - \frac{1}{\xi^5}\right)\frac{1-e^{-b\xi}}{1-R_s e^{-b\xi}}d\xi\right] \tag{8}$$

and the ratio of electron thermal conductivities in MS model is

$$\frac{\kappa_{ef}(T_e,T_l)}{\kappa_{eb}(T_l)} = \frac{T_e}{T_l}\frac{\Lambda_{e,f}(T_l)}{\Lambda_{e,b}(T_l)} = \frac{T_e}{T_l}[f(a) - g(b)\cdot I(a,b)] \tag{9}$$

with

$$\begin{aligned} &f(a) = 1 - \frac{3}{2}\frac{\phi}{a} + 3\left(\frac{\phi}{a}\right)^2 - 3\left(\frac{\phi}{a}\right)^3 1n\left(1 + \frac{a}{\phi}\right), g(b) = \frac{6(1-R_s)}{\pi b}, \\ &I(a,b) = \int_0^\pi \cos^2\theta d\theta \int_0^1 \frac{\zeta\left(1-\zeta^2\right)}{\varphi^2}\cdot\frac{1 - exp(-b\varphi/\zeta)}{1 - R_s\ exp(-b\varphi/\zeta)}d\zeta \\ &a = \frac{D}{\Lambda_{e,b}}, b = \frac{L}{\Lambda_{e,b}}, \phi = \frac{R_g}{1-R_g}, \varphi = 1 + \frac{\phi}{a\sqrt{1-\xi^2\ cos\theta}} \end{aligned} \tag{10}$$

in Eqs. (8)–(10), κ_f and κ_b denote the thermal diffusivities of film and bulk metals, respectively, a and b are the nondimensional grain diameter and film thickness, and D, L, $\Lambda_{e,b}$, R_g and R_s indicate the averaged grain diameter, the film thickness, the electron mean free path of bulk metals, the electron reflection coefficient at grain boundaries and the specular reflection coefficient of electrons at film surfaces, respectively.

In Ref. [13], a simple three-energy-level model was developed to characterize the energy exchange between electrons and the lattice and analyzes the size effect on the electron–phonon coupling factor. By considering the energy exchange of scattering between electron and phonon, the expression of electron–phonon coupling factor can be obtained as

$$G(T_e,T_l) = \frac{9}{16}\frac{nk_B^2T_D^2v_F}{\Lambda(T_l)T_lE_F} \tag{11}$$

where T_D and v_F are respectively the Debye temperature and Fermi velocity, and $\Lambda(T_l)$ is the effective electron mean free path in polycrystalline thin films [13] or stands for that of single-crystalline bulk metal [1]. From Eqs. (9)to (11), the relationship of electron–phonon coupling factor between thin metal films and bulk metals is given as

$$\frac{G_f}{G_b} = \frac{L_{e,b}}{L_{e,f}} = [f(a) - g(b)\times I(a,b)]^{-1}. \tag{12}$$

The relations (9) and (12) of MS model show that the thermal conductivity and the electron–phonon coupling factor of metal polycrystalline films are related to film thickness, grain size, surface roughness and electron reflection coefficient at grain boundaries; moreover, the effect of nonequilibrium heating greatly boosts the electron thermal conductivity because the electron temperatures are much larger than that of lattice temperatures during nonequilibrium energy transport.

3. Results and discussion

Now the governing Eqs. (1)–(4) and the prescribed conditions Eq. (6) and (7) are solved numerically by the finite element method, and thus the ultrafast thermomechanical responses of nanoscale metal films and the size effects on temperatures and thermal stresses are studied simultaneously. For quantitative analysis, an Au nanofilm of 200 nm thickness irradiated by femtosecond laser pulse is taken as an example of uniaxial strain cases. The material properties and parameters used for the calculation are given as follows [13,21]: $\rho = 19.300\ \mathrm{kg/m^3}$, $E = 74.9$ GPa, $\nu = 0.42$, $\alpha = 14.2\times10^{-6}$ nm/nmK, $C_l = 2.5\times10^6\ \mathrm{J/m^3K}$, $C_{e0} = 2.1\times10^4\ \mathrm{J/m^3K}$, $G_b = 2.6\times10^{16}\ \mathrm{W/m^3K}$, $k_{eq} = 315$ W/mK, $\tau_p = 100$ fs, $\Lambda_{e,b} = 40$ nm, $\delta = 15.3$ nm, $R_s = 0$, $R_g = 0.17$, $\beta = 2.77$, $R = 0.93$, $J = 4000\ \mathrm{Jm^{-2}}$ and $T_0 = 300$ K.

3.1. Thermophysical properties

Fig. 2 shows the size effect of grains on the thermal conductivity, electron–phonon coupling factor and thermalization time. When the average grain diameter is less than 200 nm, the size effect is evident, while it is larger than 200 nm, the size effect is negligible. When the grain size is less than the electron mean free path of gold, i.e. 40 nm, the thermal conductivity of polycrystalline Au nanofilms is much smaller than the conductivity of single-crystalline films. Hence, the grain boundary scattering increases significantly the resistance of energy transport via heat conduction. Recently Ref. [27] found that the reduction of thermal conductivities of polycrystalline Au nanofilms arose from large reflection coefficient of electrons on grain boundary which was found 0.7 or so. Hence, the effect of grain boundary scattering causes the heat conductivity of Au nanofilms to decrease one order of magnitude compared with the conductivity of Au bulk. Moreover, Ref. [27] also revealed the temperature-dependence of film thermal conductivity. For instance, when temperature increases from 80 K to 300 K, the heat conductivity would be much enhanced. MS model [13] predicts that the difference between electron temperature and lattice temperature strongly affects the heat conductivities of Au nanofilms, that is, the nonequilibrium heating effect makes the thermal conductivities increase significantly.

Similar to the case of heat conductivity, the grain boundary scattering on electron–phonon coupling factor is evident when the grain size is less than 200 nm; in particular when the grain size is less than 40 nm, the electron mean-free-path (Fig. 2). The increase of electron–phonon coupling factor with reduction of grain size greatly enhances the rate of energy exchange between electrons and phonons. Moreover, the electron–phonon coupling factor of metal nanofilms is closely related to the effect of film surface scattering [28]. Fig. 3 plots variations of the electron–phonon coupling factor with the average grain diameter for different thickness films. The electron–phonon coupling factor increases about 25% when the film thickness is reduced from 200 nm to 33 nm, since the film thickness reduction increases the scattering effects of film surfaces and grain boundaries.

The curve of thermalization time versus mean grain diameter is also displayed in Fig. 2 for crystal Au nanofilms. The thermalization time is usually defined as the time duration for electrons and the lattice to reach thermal equilibrium for typical metals. Here the thermal equilibrium means the electron temperature to be equal to the lattice temperature at the irradiative surface of Au nanofilms. For the case of small grain size, the reduction of thermalization time means that the energy exchange rate between electron and phonon is significantly enhanced. As the grain size exceeds 200 nm, the thermalization time approaches the value for the single-crystalline films. The result is different from the previous theoretic prediction given in Ref. [13]. Theoretically, the thermalization time is related with the thermophysical properties through the relation $t_c = (G/C_e + G/C_l)^{-1}$. Thus, the thermalization time is sensitive to the electron absolute temperature as indicated by $C_e = \gamma T_e$, where γ is materials constant. Compared with the predicted thermalization time 0.8 ps of Au bulk at 300 K given in Ref. [13], the thermalization time of Au nanofilms becomes one order of magnitude larger because of the size effect of grains and the nonequilibrium heating effect.

3.2. Microscale heat transport

Fig. 4 shows the size effect on the electron and lattice temperatures of Au nanofilms at three time instances of 260 fs, 10 ps and 60 ps. Owing to the size effect of grains, the temperature difference between polycrystalline films and single-crystalline film becomes evident when the grain size<40 nm. Beyond this region, the size effect becomes small and the temperature of polycrystalline Au films approaches the temperature of single-crystalline Au film. In this figure, the temperature distributions based on FS model are also plotted with dashed lines for comparison with the temperatures given by MD model. At each time

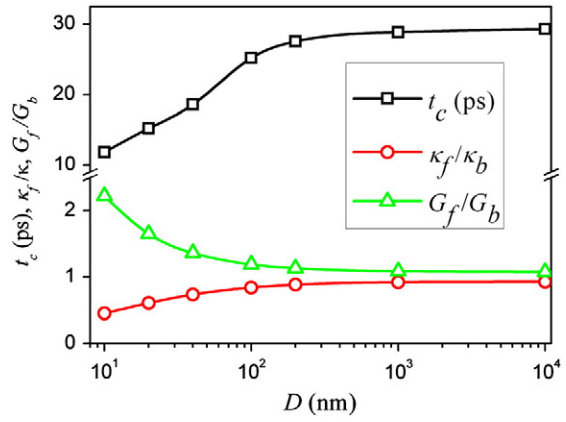

Fig. 2. Calculated grain size-dependence of thermalization time, dimensionless heat conductivity and dimensionless electron–phonon coupling factor for Au nanofilms.

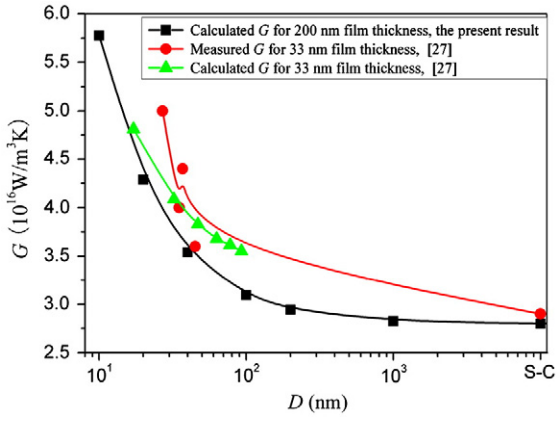

Fig. 3. Comparison of the present electron–phonon coupling factor with the results obtained in Ref. [27] for different film thickness.

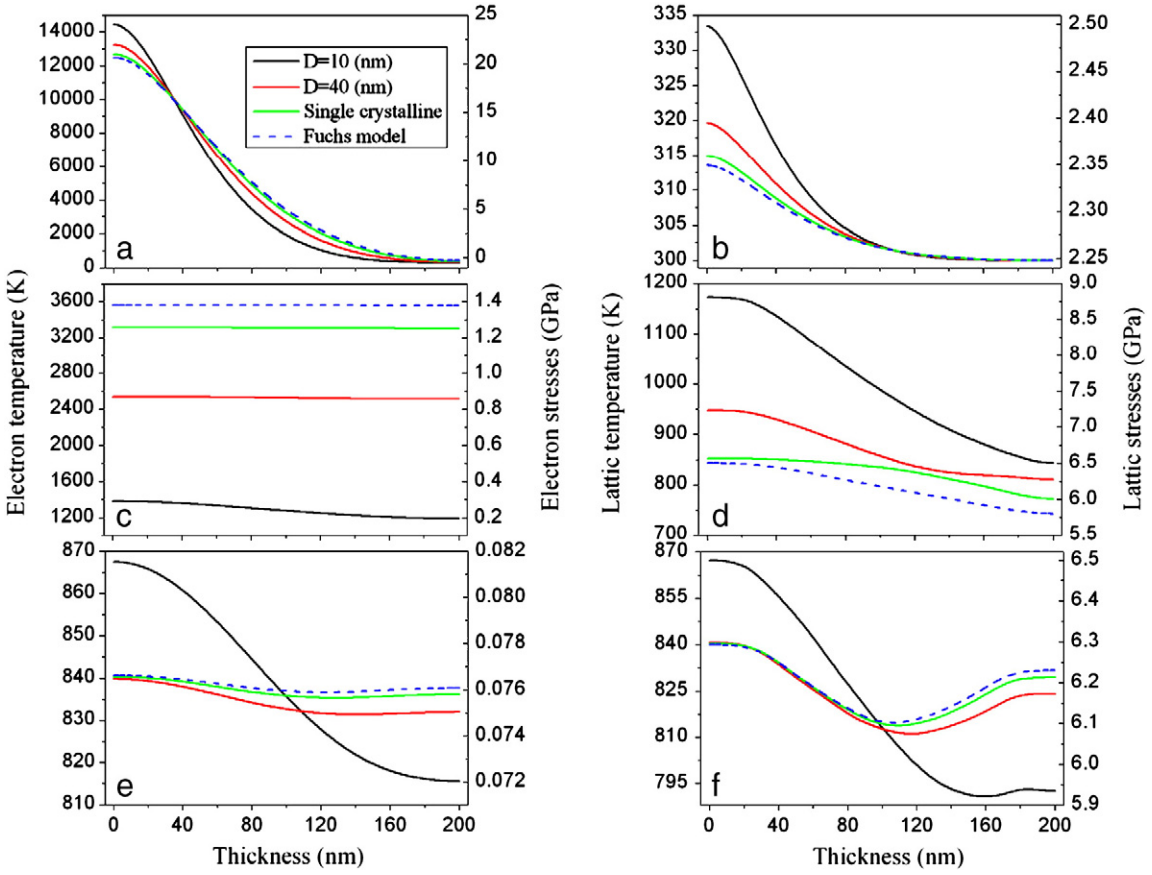

Fig. 4. The temperature distributions predicted by the two-temperature model, the FS and MS model (left vertical axis) and the stresses distributions calculated by Eq. (13) (right vertical axis) for ultrashort pulse laser heating of Au nanofilms. Corresponding times: $t = 260$ fs (*a*) and (*b*), $t = 10$ ps (*c*) and (*d*), $t = 60$ ps (*e*) and (*f*).

instances the temperatures of FS model are almost identical with the temperatures of single-crystalline film given in MS model. Only for the case of 10 ps, there is discernible difference that is less than 8%.

Fig. 4*a* and *b*shows the electron and lattice temperature distributions at 260 fs. In this case, the electron temperatures on irradiated surfaces of films reach peak values. During the laser radiating, many free electrons absorbed photon energy become excited ones at high energy levels. The excited electron energy redistributes quickly and reaches the equilibrium state with Fermi-Dirac distribution within 100 fs. This process is so fast that the electrons hardly lose energy to phonons, and thus high peak electron temperatures of the order of magnitude of 10^4 K develop at the irradiated film surfaces. For polycrystalline Au nanofilms with smaller grain size, additional grain boundary scattering would reduce heat conduction in hot electron gas. The reduction of heat conductivity leads to higher electron temperatures in the region of irradiated surface $x<40$ nm and lower electron temperatures in the internal region 40 nm$<x<$180 nm compared with the temperature of single-crystalline film. On the other hand, enhanced electron–phonon coupling factor causes high exchange rate between electron and the lattice. Hence, higher lattice temperatures in the polycrystalline Au nanofilms would develop compared with the temperature of the single-crystalline film even though the lattice temperature is only slightly enhanced. For typical metals, the Fermi velocity of electrons is typically of the order of magnitude of 10^6 m/s, much larger than the phonon–phonon energy transport speed that is about 10^3 m/s [18], which suggests that the thermal conduction in electron gas is much faster than that in the lattice. Consequently, when the electron energy propagates almost throughout the films, the lattice energy just propagates to the middle of the films.

At 10 ps, the size effect on temperature becomes more evident than that at 260 fs (Fig. 4*c* and *d*) and the grain boundary scattering has affected the entire film. In the single-crystalline film, the electron temperature reaches a temporary uniform distribution across the film thickness due to the absence of grain boundary scattering. The electron temperature is about 3500 K, while the peak lattice temperature at the irradiated film surface is about 850 K only; therefore, the electron–phonon energy exchange can proceed continuously with a high rate of $G(T_e–T_l)$ and the temporary uniform distribution of temperature will become nonuniform again. During nonequilibrium heating of Au films, there are three types of energy transports: the electron–electron heat conduction, the phonon–phonon heat conduction and the electron–phonon energy exchange. During the first 10 ps, the amount of energy transferred from irradiative surface to internal part of Au films via these three mechanisms is shown in Fig. 5*a*. Clearly, the heat conduction mechanism in hot electron gas plays the most important role in this period, and is thus the dominant that causes the electron temperature to reduce sharply and the electron energy to tend to uniform distribution in the single-crystalline film. For a 40 nm crystal film, the time period of 10 ps is far from its thermalization time of 18.6 ps and the nonequilibrium energy transport process would take place. Therefore, enhanced electron–phonon energy exchange and reduced electron heat conduction result in lower electron temperature and higher lattice temperature compared with those of single-crystalline film. For a 10 nm crystal film, the time 10 ps is close to the thermalization time 11.8 ps and the temperatures between electrons and the lattice have nearly reached thermal equilibrium. The total amount of electron–phonon energy exchange, that is the integral area under the curves $G(T_e–T_l)$ in Fig. 4*b*, is the largest in the film. Hence, the significant reduction of

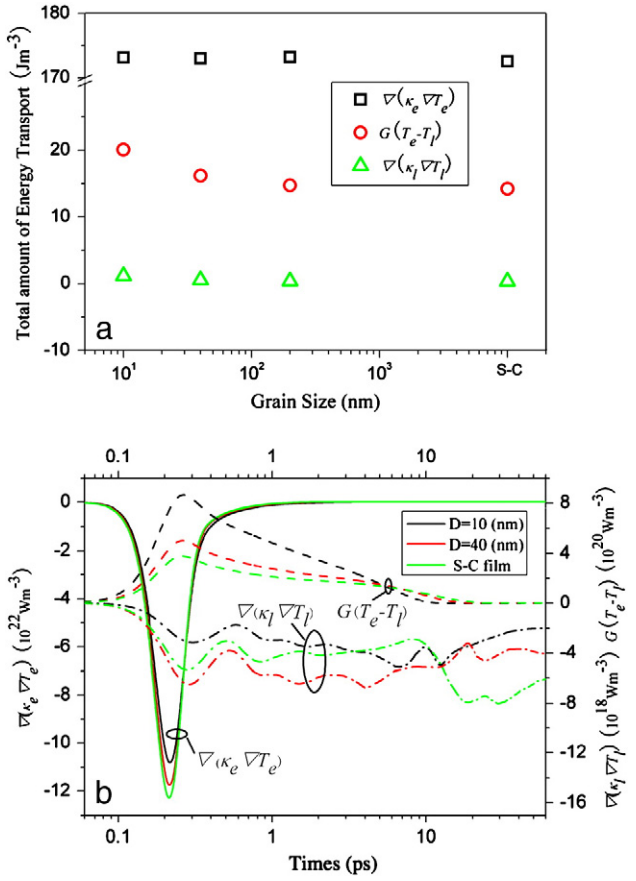

Fig. 5. *a*. Total amount of energy transport by heat conductions in electron gas and the lattice and the amount of electron–phonon energy exchange during the first 10 ps. *b*. Rates of energy transport occurring at the film radiative surface contributed by heat conduction in electrons and in the lattice as well as the electron–phonon energy exchange during the interval of 60 ps.

electron temperature and enhancement of lattice temperature result in the lowest electron temperature and the highest lattice temperature.

Fig. 4*e* and *f*shows the temperature distributions of films at 60 ps. After electron–phonon energy equilibrium is established, phonons become the main energy carriers and carry much more energy as compared with electrons. The calculation of energy transport rates (Fig. 4*b*) shows that the heat conduction in phonon has become the dominative mechanism of energy transport during thermal equilibrium, in which the heat conduction in electrons and the electron–phonon energy exchange have finished and the rates of energy transport in polycrystalline films is smaller than that in single-crystalline film. Therefore, both the electron and lattice temperatures in a 10 nm crystal film would reduce very slowly so that the highest temperature gradient would develop across the film thickness. For the single-crystalline film, due to the absence of grain boundary scattering, relative quick heat conduction process causes the evolution of energy towards uniform distribution across the film thickness. For a 40 nm polycrystalline film, the reduction of heat conductivity and the enhancement of electron–phonon coupling factor compared with the single-crystalline film are small (Fig. 2). Therefore, the energy distribution approaches the energy state of single-crystalline film. In comparing the electron and lattice temperatures in Fig. 3*e* and *f*, we notice a discernible difference in the curve shape between the electron and lattice temperatures. The difference is caused by the thermal expansion effect of lattice volume $(3\lambda+2\mu)\alpha T_l(d\varepsilon_{kk}/dt)$ in the lattice energy balance condition of Eq. (2).

Both experimentally measured [3] and theoretically predicted [13] heat propagation speeds in hot electron gas of Au bulk are around 8×10^5 m/s, while the speed in the crystal Au nanofilms is reduced to 5×10^5 m/s since the size effect greatly decreases the thermal conductivity. Therefore, the propagation distance of electron heat waves at time 260 fs is about 140 nm as shown in Fig. 4*a*. From phonon energy balance Eq. (2), the heat wave speed in the lattice is found to be $c_l=(\kappa_l/\tau_l C_l)^{1/2}=1775$ m/s in Au bulk with phonon–phonon scattering time $\tau_l=38$ ps [18], and thus the phonon heat wave just propagates a distance of 0.462 nm at 260 fs. This propagation distance is evidently different from the calculated results shown in Fig. 3*b*. The difference of heat wave propagation distance suggests that the ultrafast laser heating induces two heat waves in the lattice. A slow wave with propagation speed of 1775 m/s is generated by the phonon–phonon scattering with relaxation time τ_l, and a fast wave propagating at a quite high speed is associated with the electron–electron scattering and electron–phonon interaction. During ultrafast laser heating of metals, the phonon obtaining energy from excited electrons involves two relaxation times: the electron–electron scattering time τ_e of about 10–50 fs and the electron–phonon scattering time τ_{ep} of about 100 fs for Au bulk at 300 K [25]. The electron–phonon scattering effect causes a delay of electron–phonon scattering time in the phonon fast wave propagation compared with the electron heat wave. Based on theoretic predicted electron–phonon coupled factor (Fig. 2), the electron–phonon scattering time is in the range from 45 fs to 73 fs for crystal Au nanofilms. Since electron–electron scattering and electron–phonon scattering occur one after another, we can assume that the effective relaxation time is the sum of their scattering time, that is, $\tau_{eff}=\tau_e+\tau_{ep}$. By using electron heat wave Eqs. (1) and (2), the fast wave speed can be defined as $c_p=(\kappa_e/\tau_{eff}C_e)^{1/2}$ and its value is found to be 2.87×10^5 m/s. With this speed value, the propagation distance of the phonon fast wave is about 74.62 nm at 260 fs. This distance agrees with the calculated results given in Fig. 3*b*. In physics, the fast wave reflects the propagation characteristics of electron–phonon interaction, a heat source moving with high speed. Therefore, the dynamic behaviors of fast wave depend on the electron heat wave traits and the electron–phonon energy exchange rate. As stated in Section 2, the governing equations of the fast wave consist of energy balance condition Eq. (2) and the modified Cattaneo's thermal constitutive model. The detail in deriving the governing equations of fast wave will be provided in other papers.

3.3. Ultrafast mechanical responses

Fig. 6*a*–*c*shows the size-dependent stress distributions of the Au nanofilms at three time instances: the time of 260 fs at which the deposition of radiation energy on electrons tends to complete, the nonequilibrium heating time of 10 ps at which the maximum normal compressive stress develops in Au films, and the equilibrium heating time of 60 ps at which the maximum normal tensile stress develops in Au films. At present, these stresses are calculated based on classical thermoelastic theory, that is, the thermal stresses are caused by the lattice temperature change as shown in Eq. (3). Hence, the size effect on the stresses is analogous to the size effect on the lattice temperatures. The less the grain mean diameter, the more evident the size effect. Similarly, when the grain size is less than electron mean free path 40 nm, the size effect becomes quite evident, and the larger the lattice temperature gradient (Fig. 4*b*), the greater the stress magnitude (Fig. 6*a*). Owing to gradual decrease of temperature gradients, the greatest stress is built up in the 10 nm polycrystalline film; the secondary large stress develops in the 40 nm crystal film, and the smallest stress in the single-crystal film. Since the temperature gradients calculated based on FS and MS models are almost identical (Fig. 4), the stress difference between the two models is small as well.

During the deposition of radiation energy on electrons, free electrons momentarily reach a much higher temperature than the lattice temperature. This process is too fast for the electrons to

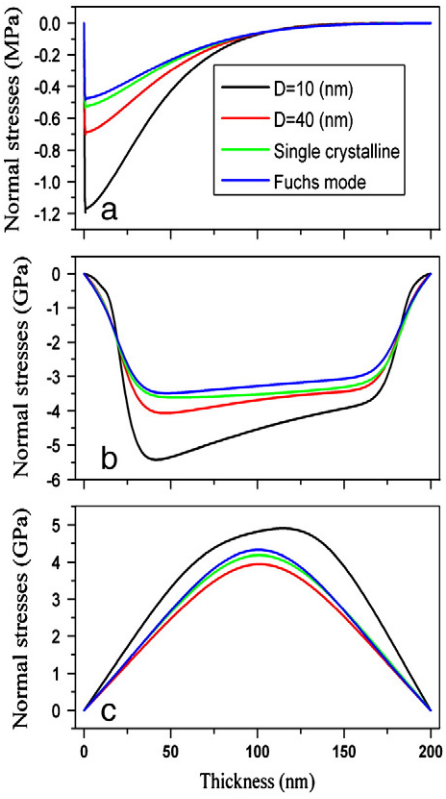

Fig. 6. Predicted normal stress distributions developed in Au nanofilms at the time of (*a*) $t=260$ fs, (*b*) $t=10$ ps and (*c*) $t=60$ ps.

transfer energy to other energy carriers by conduction. A majority of energy depositing on Au nanofilm builds up in the radiation penetration depth to form a laminar region with high energy density. Logically, the extremely nonuniform distribution of energy should generate quite large stresses in the radiation region, that is to say, the contribution of electron temperature to the stress could be more important compared with the lattice temperature contribution in the period of 260 fs. However, the stress magnitudes (Fig. 6*a*) are merely in the order of MPa. The stresses are small in magnitudes, since the lattice temperatures increase slightly and the classical thermoelastic theory doesn't take into account the nonequilibrium heating effect. When electrons and the lattice are not in thermal equilibrium, the classical thermoelastic theory can't describe generation and evolution of the stress. The microscopic process of generation of nonequilibrium stresses is related to the instantaneous temperature change of electrons and the lattice [19] and can be described by:

$$s = -g_e C_e \mathrm{D}T_e - g_l C_l \mathrm{D}T_l \tag{13}$$

where C_e, γ_e and C_l, γ_l refer to the specific heat capacities per unit volume and the average Grüneisen parameters for the electron and phonon subsystems. Eq. (13) shows that the stresses of Au nanofilms are caused by the thermal pressure of electrons and the lattice anharmonicity, respectively. Since the contribution of electron temperature to the stress is included, the nonequilibrium heating effect can now be considered. Fig. 4 illustrates the stress distributions calculated from Eq. (13). From depositing radiative energy on electrons to establishing electron–lattice thermal equilibrium, the electric thermal stresses decrease from 25 GPa to 75 MPa (Fig. 4*a*, *c* and *e*), while the lattice thermal stresses increase from 2.5 GPa to 6.2 Gpa (Fig. 4*b*, *d* and *f*). Therefore, during the deposition of radiative energy on electrons, the electron temperatures play a dominant role in stress generation, that is to say, the nonequilibrium effect on stress is very important. In the later period of nonequilibrium heating and thermal equilibrium, the lattice temperature becomes a dominant factor for the enhancement of film stresses. Note that the nonequilibrium stresses do not comply with the classical thermoelastic theory because both the stresses related to the electron temperature and that related to the lattice temperature (Fig. 4*a*–*d*) are several orders of magnitude higher than the thermoelastic stresses (Fig. 6*a*). In thermal equilibrium, the thermoelastic stresses, such as the maximum compressive stresses developed at the time of 10 ps (Fig. 6*b*) and the maximum tensile stresses developed at the time of 60 ps (Fig. 6*c*), are close in magnitude to the equilibrium stresses obtained from Eq. (13) (Fig. 4*f*). Consequently, the thermoelastic theory is suitable for the description of thermal equilibrium stresses.

The discussion above shows that Eq. (13) describes the generation of ultrafast stresses in nonequilibrium heating of metal nanofilms. However, the relationship can not reveal the propagation characteristics of ultrafast stress waves, and thus studying the problem requires the atom or lattice model [20,29]. Moreover, the electron stress reaches 25 GPa at 260 fs (Fig. 4*a*), a value much greater than the strength of Au bulk of 1.24 GPa, which implies that non-ablation failure of Au nanofilms is likely to occur during the deposition of radiative energy on electrons. These problems will be studied in depth in the future.

4. Conclusions

In summary, the thermomechanical responses and the grain boundaries scattering induced by femtosecond pulse laser in Au nanofilms has been investigated by using two-temperature model and Cattaneo's thermal constitutive equation. The size-dependence of thermophysical properties becomes evident when the average grain diameter is less than the film thickness. In addition to the scattering of grain boundaries, the nonequilibrium heating effect is also a dominant factor in the prolongation of thermalization time. The grain scattering as a microscale energy transport mechanism becomes important when the grain size is comparable to or smaller than the mean free path of the conduction electrons. The study on heat transport mechanisms shows that there are two heat waves propagating in the lattice during nonequilibrium heating of films. The propagation characteristics of slow wave are related only with the phonon–phonon scattering mechanisms, but the fast wave characteristics depend on both the electron heat wave propagation and the electron–phonon interaction. The result of the ultrafast dynamic responses suggests that Eq. (13) can describe the generation of ultrafast stresses involving nonequilibrium effect, while the classical thermoelastic theory can approximately describe the stress evolution in the stage of thermal equilibrium.

Acknowledgments

The project was supported by the National Natural Science Foundation of China (10672166, 10632100).

References

[1] M.I. Kaganov, I.M. Lifshitz, L.V. Tanatarov, Sov. Phys. JETP. 4 (1957) 173.
[2] S.I. Anisimov, B.L. Kapeliovich, T.L. Perel'man, Sov. Phys. JETP. 39 (1974) 375.
[3] G.L. Eesley, Phys. Rev. Lett. 51 (1983) 2140.
[4] S.D. Brorson, J.G. Fujimoto, E.P. Ippen, Phys. Rev. Lett. 59 (1987) 1962.
[5] T.Q. Qiu, C.L. Tien, J. Heat Transfer. 115 (1993) 835.
[6] K. Fuchs, Proc. Camb. Philos. Soc. 34 (1938) 100.
[7] E.H. Sondheimer, Adv. Phys. 1 (1952) 1.
[8] A.F. Mayadas, M. Shatzkes, Phys. Rev. B. 1 (1970) 1382.
[9] A.F. Mayadas, J. Appl. Phys. 39 (1968) 4241.
[10] A.L. Lima, X. Zhang, A. Misra, C.H. Booth, E.D. Bauer, M.F. Hundley, Thin Solid Films 515 (2007) 3574.
[11] J.M. Camacho, A.I. Oliva, Thin Solid Films 515 (2007) 1881.
[12] H. Marom, M. Ritterband, M. Eizenberg, Thin Solid Films 510 (2006) 62.

[13] T.Q. Qiu, C.L. Tien, ASME J. Heat Transfer. 115 (1993) 842.
[14] W. Steinhögl, G. Schindler, G. Steinlesberger, M. Engelhardt, Phys. Rev. B. 66 (2002) 075414.
[15] C. Durkan, M.E. Welland, Phys. Rev. B. 61 (2000) 14215.
[16] M.I. Flik, C.L. Tien, ASME J. Heat Transfer. 112 (1990) 872.
[17] L.H. Liang, B. Li, Phys. Rev. B. 73 (2006) 153303.
[18] C. Kittel, Introduction to Solid State Physics, Wiley, New York, 1986.
[19] O.B. Wright, Phys. Rev. B. 49 (1994) 9985.
[20] J. Tang, Appl. Phys. Lett. 92 (2008) 011901.
[21] Y. Gan, J.K. Chen, Appl. Phys. Lett. 94 (2009) 201116.
[22] D.D. Joseph, L. Preziosi, Rev. Mod. Phys. 61 (1989) 41.
[23] D.D. Joseph, L. Preziosi, Rev. Mod. Phys. 62 (1990) 375.
[24] J. Chen, I.V. Tomov, H.E. Elsayed-Ali, P.M. Rentzepis, Chem. Phys. Lett. 419 (2006) 374.
[25] C.L. Tien, A. Maiumdar, F.M. Gerner, Microscale Energy Transport, Taylor & Francis, Washington, 1988.
[26] C. Cattaneo, C. R. Acad. Sci. 247 (1958) 431.
[27] Q.G. Zhang, B.Y. Cao, X. Zhang, Phys. Rev. B. 74 (2006) 134109.
[28] J.L. Hostetler, A.N. Simith, D.M. Czajkowsky, P.M. Norris, Appl. Optics 38 (1999) 3614.
[29] J. Li, R. Clinite, X. Wang, J. Cao, Phys. Rev. B. 80 (2002) 014304.